communications biology

Article

https://doi.org/10.1038/s42003-024-07049-w

Alternative sources of molybdenum for *Methanococcus maripaludis* and their implication for the evolution of molybdoenzymes

Check for updates

Devon Payne[1], Lisa M. Keller[1], James Larson[2], Brian Bothner[2], Daniel R. Colman[1] & Eric S. Boyd[1]

Molybdoenzymes are essential in global nitrogen, carbon, and sulfur cycling. To date, the only known bioavailable source of molybdenum (Mo) is molybdate. However, in the sulfidic and anoxic (euxinic) habitats that predominate in modern subsurface environments and that were pervasive prior to Earth's widespread oxygenation, Mo occurs as soluble tetrathiomolybdate ion and molybdenite mineral that is not known to be bioavailable. This presents a paradox for how organisms obtain Mo to support molybdoenzymes in these environments. Here, we show that tetrathiomolybdate and molybdenite sustain the high Mo demand of a model anaerobic methanogen, *Methanococcus maripaludis*, grown via Mo-dependent formate dehydrogenase, formylmethanofuran dehydrogenase, and nitrogenase. Cells grown with tetrathiomolybdate and molybdenite have similar growth kinetics, Mo content, and transcript levels of proteins involved in Mo transport and cofactor biosynthesis when compared to those grown with molybdate, implying similar mechanisms of transport and cofactor biosynthesis. These results help to reconcile the paradox of how Mo is acquired in modern and ancient anaerobes and provide new insight into how molybdoenzymes could have evolved prior to Earth's oxygenation.

Metals are the catalytic components of many enzymes, including those requiring iron (Fe), nickel (Ni), and/or molybdenum (Mo), among others[1]. Currently, Mo is the most abundant trace element in modern oceans (~100 nM) as molybdate ion (MoO_4^{2-})[2,3] due to the oxygen (O_2)-dependent oxidative weathering of molybdenite (MoS_2) and other Mo-bearing minerals in the Earth's crust[4]. As such, prior to the Great Oxidation Event (GOE) ~ 2.4 Gya, the delivery of MoO_4^{2-} to aquatic environments would have been limited[5] and it has been suggested that Mo-dependent enzymes are unlikely to have evolved prior to the advent of oxygenic photosynthesis[6]. Many biological nitrogen cycling activities are dependent on Mo-dependent enzymes and MoO_4^{2-} limitation prior to the GOE is thought to have limited these activities that, in turn, would have constrained the productivity of microbial ecosystems[3,5,7]. Yet, several studies implicate the Last Universal Common Ancestor as being Mo-dependent[8]. The origin and function of Mo-dependent enzymes during the Archean when MoO_4^{2-} was limiting in aquatic environments is enigmatic and is referred to as the "Mo paradox"[9,10].

Two groups of Mo-dependent metalloenzymes have been described: i) molybdenum nitrogenase (Nif) that hosts a Mo-containing cofactor that comprises Fe, sulfur (S), carbon, and homocitrate[11], also known as FeMo-co[12], and ii), all other "molybdoenzymes" where Mo is bound to a pterin cofactor (molybdopterin or Mo-co)[13,14]. Homologs of both types of molybdoenzymes have been identified in Archaea and Bacteria, including aerobes, anaerobes, chemotrophs, and phototrophs[15,16]. Methanogens are obligate anaerobes that can require both FeMo-co and Mo-co, contingent on growth conditions. For example, the activity of formylmethanofuran dehydrogenase (Fmd), which catalyzes the first step of hydrogenotrophic methanogenesis and the Wood-Ljungdahl (WL) pathway of CO_2 fixation, is dependent on Mo-co although it has been shown that tungsten (W) can substitute during Mo limitation[14,17,18]. Similarly, the activity of formate dehydrogenase (Fdh), which catalyzes the oxidation of formate to CO_2 and hydrogen (H_2) during formate-dependent methanogenesis, is also dependent on Mo-co[19,20]. In addition to Mo-co-containing enzymes, many methanogens encode Nif that catalyzes the reduction of dinitrogen (N_2) into bioavailable ammonia (NH_3), with substrate reduction occurring at FeMo-co[21,22]. WL-encoding hydrogenotrophic methanogens evolved early in Earth's history[23–25] and are the likely lineage where Nif first originated[1,26].

[1]Department of Microbiology and Cell Biology, Montana State University, Bozeman, MT, USA. [2]Department of Chemistry and Biochemistry, Montana State University, Bozeman, MT, USA. e-mail: eric.boyd@montana.edu

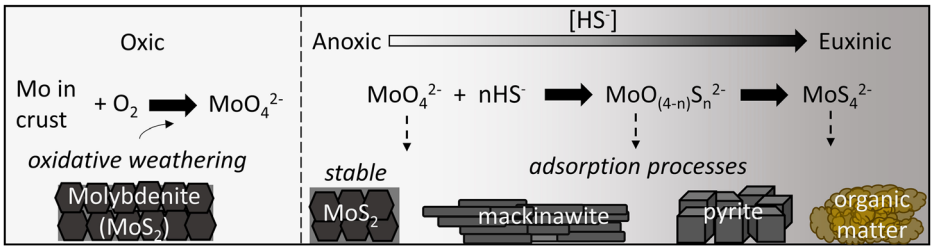

Fig. 1 | The sources, sinks, and speciation of molybdenum (Mo) in oxic and euxinic aquatic environments. In oxic aquatic environments, oxidative weathering of Mo in crustal minerals such as molybdenite (MoS_2) can lead to the release of soluble molybdate (MoO_4^{2-}) ions. Molybdate that is introduced to anoxic aquatic environments is generally stable unless sufficient sulfide (HS^-) is present to react and form thiomolybdate species ($MoO_{(4-n)}S_n^{2-}$) such as tetrathiomolybdate (MoS_4^{2-}) that can adsorb onto organic matter or the surfaces of iron-sulfide minerals such as mackinawite (FeS) and pyrite (FeS_2) (as reviewed in ref. 30).

As such, methanogens are ideal model organisms to study Mo acquisition in modern anaerobes with implications for how Mo was acquired for use in the biosynthesis of early evolving molybdoenzyme cofactors.

The typical source of Mo used to cultivate methanogens is MoO_4^{2-}, whereas the typical source of S to cultivate methanogens is sulfide (HS^-), presumably because these organisms often inhabit sulfidic or euxinic environments[27,28]. However, HS^- readily reacts with MoO_4^{2-}, resulting in the progressive replacement of oxygen atoms with S atoms, finally resulting in the formation of soluble tetrathiomolybdate (MoS_4^{2-})[29]. MoS_4^{2-} can then adsorb to organic matter or iron-sulfide mineral phases (i.e., mackinawite (FeS_{mack}) and pyrite (FeS_2)) that can lead to incorporation of Mo as a heterometal in those minerals (Fig. 1)[29–33]. Indeed, it has previously been shown that the 2 mM concentration of HS^- typically used to cultivate methanogens reacted quickly with MoO_4^{2-} to form MoS_4^{2-}[28]. Despite the high levels of HS^- used to cultivate methanogens, many studies have demonstrated methanogen growth under conditions requiring Fdh, Fmd, and Nif when provided with MoO_4^{2-} as the sole Mo source [28,34].

Recently, *Methanococcus maripaludis* S2 was grown with formate as methanogenesis substrate under nitrogen-fixing (diazotrophic) conditions to impart a high Mo demand on cells[28]. Cells were grown in cultivation medium amended with either excess ferrous iron (Fe(II)) or excess HS^- to mimic ferruginous conditions on early Earth or the euxinic conditions that likely predominated in the early Proterozoic, respectively. Euxinic conditions inhibited diazotrophic growth relative to ferruginous conditions, and far less MoO_4^{2-} was required to meet cell demands in ferruginous conditions. This suggests that HS^- was influencing the speciation and availability of Mo and raises the question as to whether thiolated forms of Mo can support growth of methanogens (and other anaerobes). Here, we tested whether the anaerobe *M. maripaludis* S2 can grow formatotrophically (requires Fdh, Fmd) and diazotrophically (requires Nif) with soluble MoS_4^{2-} and MoS_2 mineral by quantifying growth kinetics, transcriptional responses, and biomass Mo content in cells when compared to those grown with MoO_4^{2-}. The results are used to reconcile the paradox of how Mo is acquired in modern and ancient anaerobes and their implications for how molybdoenzymes could have evolved prior to Earth's oxygenation.

Results

Growth of *M. maripaludis* with alternative soluble molybdenum sources

To test growth of *M. maripaludis* with alternative Mo sources, a source(s) of S (other than HS^-) was first identified that can support growth and that avoided confounding experimental outcomes due to thiolation of MoO_4^{2-}. L-cysteine alone (2 mM) or a combination of L-cysteine and thiosulfate at 1 mM concentration each supported growth and, importantly, did not support growth in the absence of N_2 or NH_3 indicating they cannot serve as sole nitrogen source (Supplementary Results; Figs. S1–S3). In addition, other components of the growth medium (e.g., source of Fe, trace metal concentrations) affected the availability of the supplied Mo source as determined by UV-Vis spectroscopy (Supplementary Figs. 4 and 5). As such, experiments were performed to optimize medium conditions to promote the availability and stability of MoS_4^{2-}. Cultures provided with 10-fold less trace metals maintained robust growth (relative to those provided with canonical concentrations of trace metals) and cultures provided with FeS_{mack} grew as well as those grown with ferrous chloride ($FeCl_2$). Both of these conditions (0.1 X trace elements and replacement of $FeCl_2$ with FeS_{mack}) allowed MoS_4^{2-} to stay in solution longer (described in more detail below). We performed a catechol assay, which is specific to MoO_4^{2-}[28], in the MoS_4^{2-} reactors and found no evidence of MoO_4^{2-} indicating that it was not oxidized under these conditions.

M. maripaludis was therefore passaged several times in medium with L-cysteine and thiosulfate (CT conditions; 1 mM of each) as S sources, 0.1 X the concentration of trace elements typically used to cultivate *M. maripaludis*[28], and with FeS_{mack} as the Fe source under N_2 fixing conditions with formate as methanogenesis substrate. No Mo was provided to CT-grown cells to generate Mo-limited cells. However, despite attempts to reduce background Mo in cultivation medium, including preparing medium with nitric acid-washed plastic utensils/containers and using trace metal grade water, cultures never reached full Mo limitation to the extent that no growth was observed. Nonetheless, a significant reduction in growth rate was observed in cultures not provided with Mo compared to those provided with Mo (as in ref. 28, which is further assessed through much more robust experimentation reported below. This provided a phenotype that allowed for experiments comparing the influence of Mo source on cell growth and activity to proceed.

Cells grown in CT conditions were washed to remove carryover metals and were then used as inoculum for medium containing either 5 μM $Na_2MoO_4^{2-}$ as a positive control (abbreviated as "MoO_4^{2-}"), 5 μM ammonium tetrathiomolybdate ($(NH_4)_2MoS_4$) as the experimental treatment (abbreviated as "MoS_4^{2-}"), or with no Mo added (abbreviated as "no Mo") as a negative control to account for contaminant Mo under nitrogen-fixing conditions with formate as methanogenesis substrate. A control culture amended with 10 μM NH_4Cl but without Mo was also included to account for any stimulatory effect that ammonium in the $(NH_4)_2MoS_4$ stock could have when provided to cells. Production of cells and CH_4 were observed in all culture conditions (Fig. 2A and B). Cultures provided with MoS_4^{2-} exhibited the shortest lag phase and reached slightly higher cell densities than cultures provided with MoO_4^{2-}. Cultures not provided with Mo either with or without 10 μM NH_4Cl grew significantly slower than cultures provided with MoO_4^{2-} or MoS_4^{2-} (Fig. 2C), and the addition of 10 μM NH_4Cl had a minute stimulatory effect on cultures not provided with a Mo source (Fig. 2A and B). The stronger growth response in cultures provided with 5 μM Mo, regardless of source, versus no Mo controls indicates that Mo is not toxic at these levels, consistent with past reports[28].

UV-vis spectroscopy was used to qualitatively assess MoS_4^{2-} stability in the cultures provided with MoO_4^{2-}, MoS_4^{2-}, or no Mo (Fig. 2D). In cultures provided with MoS_4^{2-}, the intensity of MoS_4^{2-} peaks (318 and 468 nm) diminished by ~50% in the first 20 h. of incubation and by 70% after 40 h. of incubation. There was no evidence of conversion of MoS_4^{2-} to intermediate thiomolybdate species ($MoO_{(4-n)}S_n^{2-}$; absorbance peaks at ~396 nm[29,35]), which would be expected if MoS_4^{2-} was being oxidized. Similarly, UV-vis spectroscopy of cultures amended with MoO_4^{2-} or no Mo did not show evidence for the presence of $MoO_{(4-n)}S_n^{2-}$ species (Fig. 2D). Together, these

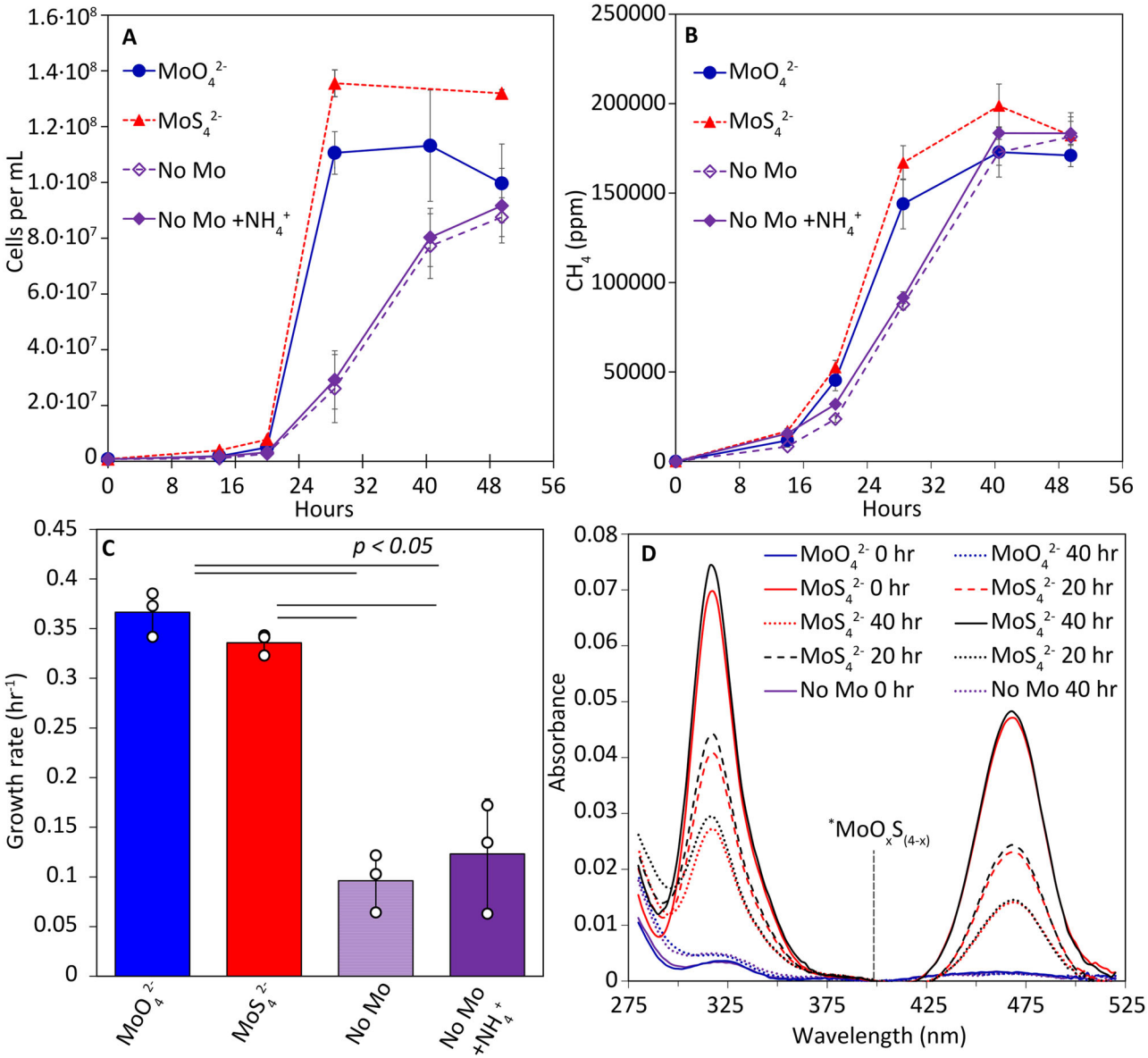

Fig. 2 | Growth of *Methanococcus maripaludis* S2 on soluble sources of molybdenum (Mo) under nitrogen-fixing cultivation conditions. The production of cells (**A**) and methane (CH_4; **B**) were tracked over time in cultures grown with 1 mM each L-cysteine and thiosulfate as the sulfur source and formate as the methanogenesis substrate. Cells were provided with 5 µM molybdate (MoO_4^{2-}; blue circles), 5 µM ammonium tetrathiomolybdate ($(NH_4)_2MoS_4$; red triangles), or no Mo with 10 µM ammonium chloride (NH_4^+; closed purple diamonds; added to account for NH_4^+ in $(NH_4)_2MoS_4$) or without NH_4Cl (open purple diamonds). Maximum growth rates were calculated for each condition (**C**). UV-vis spectroscopy was used to track MoS_4^{2-} concentration and speciation over time in 0.2 µm-filtered samples, with a vertical dashed line denoting where intermediate thiomolybdate species ($MoO_xS_{(4-x)}$) absorbance would occur (**D**). A standard curve for MoS_4^{2-} absorbance at 468 nm is shown in Supplementary Fig. 5. Data shown are the mean and standard deviation of three biological replicates; a single abiotic reactor (black traces) was used for (**D**). *p*-values are the result of two-tailed Student's *t*-tests.

data indicate that the decrease in the MoS_4^{2-} signal in reactors is due to its assimilation into biomass and/or adsorption or complexation with FeS_{mack} or other components of the medium including copper, consistent with its well-known affinity towards such compounds[33,35], rather than due to oxidation.

The effect of 1 mM HS^- on cultures of *M. maripaludis* grown with MoS_4^{2-} was examined and was found to support higher growth efficiencies than the no Mo negative control (Supplementary Fig. 6). The sulfidic conditions tested are expected to favor thiolated MoS_4^{2-} species[28,29], providing additional support for its use by *M. maripaludis*. Together, these results indicate that the speciation of the Mo sources tested remained largely unchanged during the incubation and that the Mo sources provided remained soluble and available during growth. These data, combined with the differences in growth rates (Fig. 2C) and maximum cell densities (Fig. 2A) between no Mo control cultures and the MoO_4^{2-} and MoS_4^{2-}-amended cultures, provide clear indication that *M. maripaludis* can utilize MoS_4^{2-} as well, if not better, than MoO_4^{2-}.

Mo content of cell biomass

To further investigate the bioavailability and use of MoS_4^{2-} by nitrogen-fixing and formate-grown *M. maripaludis* cells, cultures grown on the different Mo sources were harvested at late-log phase to determine biomass Mo content. Harvested cells were washed to remove metals loosely associated with biomass as well as to remove residual metal in the supernatant. The resulting cell pellets were dried and subsequently dissolved in trace metal grade nitric acid and the metal content was determined by inductively

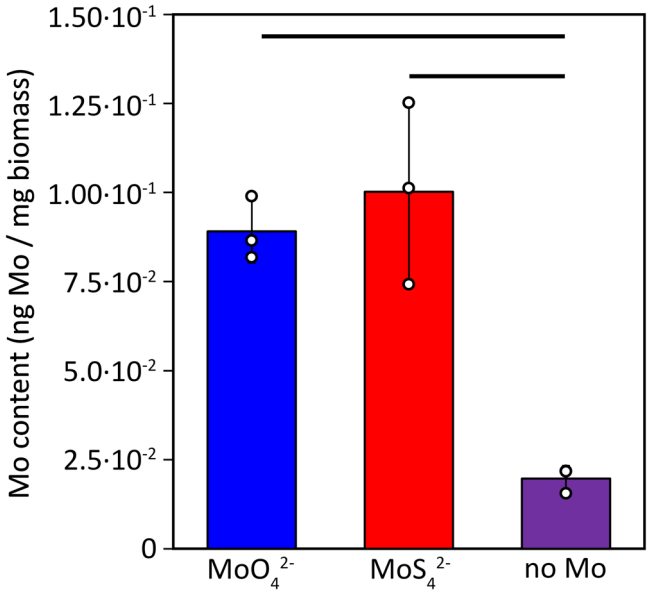

Fig. 3 | Molybdenum (Mo) content of *Methanococcus maripaludis* S2 cells grown on different Mo sources under nitrogen-fixing cultivation conditions. *M. maripaludis* was grown with 5 μM molybdate (MoO_4^{2-}), 5 μM tetrathiomolybdate (MoS_4^{2-}), or no Mo (no Mo). Cells were washed three times with nitriloacetic acid prior to whole-cell metal analysis by inductively coupled plasma emission-mass spectrometry. Data shown are the mean and standard deviation of three biological replicates for each condition. Bars above the plot indicate statistical significance at $p < 0.05$ in a two-tailed Student's *t*-test; the absence of a bar indicates a *p*-value of > 0.05.

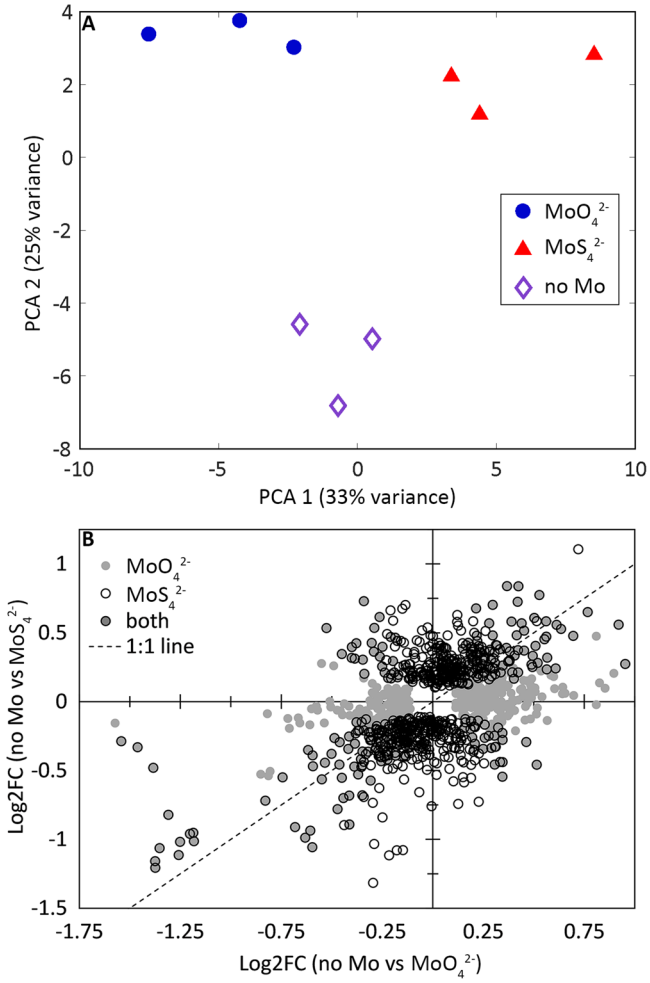

Fig. 4 | Transcriptomic profiles for *Methanococcus maripaludis* S2 cells grown on different molybdenum (Mo) sources under nitrogen-fixing cultivation conditions. Principal component analysis of *M. maripaludis* transcriptomic profiles of cells grown with molybdate (MoO_4^{2-}, blue circles), tetrathiomolybdate (MoS_4^{2-}, red triangles), or no Mo provided (purple diamonds) (**A**). The variance loadings (as a percentage) on each of the first two principal component axes (PCA) are indicated. Significant differential gene expression ($p < 0.05$, Wald test) relative to no Mo controls are shown for cells provided with MoO_4^{2-} (x-axis) and MoS_4^{2-} (y-axis) with each point representing an individual gene (**B**). Transcriptional profiles in B are the mean expression of three replicate cultures. A volcano plot of expression profiles for cells grown with MoO_4^{2-} versus MoS_4^{2-}, with locus tags of significantly differentially expressed genes, is presented in Supplementary Fig. 7. Fold-induction (log_2fold change) values for pairwise treatment comparisons or normalized gene expression (rlog) and variance stabilizing transformation (vst) values for each individual treatment are presented in Supplementary Dataset 1.

coupled plasma mass spectrometry (ICP-MS). The Mo content per mg biomass in MoO_4^{2-}- and MoS_4^{2-}-grown cells was similar whereas cells provided with no Mo (negative control) had ~80% less Mo per mg biomass (Fig. 3). Thus, the defect in the kinetics of cell production in cultures not provided with Mo (no Mo; Fig. 2A, C) is attributed to a deficiency in available Mo. The similar Mo content of cells grown with MoO_4^{2-} versus MoS_4^{2-} implies similar bioavailability and/or similar efficiency in acquiring and trafficking these anionic forms of Mo in *M. maripaludis* cells.

Differential gene expression of cells grown on soluble Mo sources

Patterns of gene expression in *M. maripaludis* cultures grown with MoO_4^{2-} versus MoS_4^{2-}, as well as cultures not provided with a Mo source (no Mo; negative control), were compared using RNA-seq. Cells exhibited markedly different transcriptional profiles when provided with MoO_4^{2-}, MoS_4^{2-}, or with no Mo source as indicated by clustering of transcriptomes of each of the three conditions in a principal coordinate ordination (PCO; Fig. 4A). Transcriptomes of MoO_4^{2-}- versus MoS_4^{2-}-grown *M. maripaludis* cells separated along PCO Axis 1 (33% of variance explained) while those of MoO_4^{2-}- and MoS_4^{2-}-grown cells separated from cells not provided with Mo (no Mo) along PCO Axis 2 (25% of variance explained). When compared to cultures not provided with a Mo source (no Mo), 979 genes of the 1,793 annotated genes in the *M. maripaludis* genome (~55%) were differentially regulated ($p < 0.05$, Wald test) in MoO_4^{2-}- or MoS_4^{2-}-grown cultures (Fig. 4B; Supplementary Fig. 7)). Specifically, 599 genes were differentially regulated in cells provided with MoO_4^{2-} versus those provided with no Mo, 673 genes were differentially regulated in cells provided with MoS_4^{2-} versus those provided with no Mo, and 293 genes were differentially regulated in cells provided with either MoO_4^{2-}- or MoS_4^{2-} versus those provided with no Mo. A comparison of these genes shows significant spread and opposing regulation (deviation from 1:1 line) based on the Mo source provided (Fig. 4B, Supplementary Fig. 8). Notably, genes encoding flagella were found to be among the most up-regulated genes in cells provided with either MoO_4^{2-} or MoS_4^{2-} relative to cells provided with no Mo, indicating that Mo availability impacts the regulation of motility. Many of the other genes that were differentially regulated in MoO_4^{2-}- and MoS_4^{2-}-grown cells relative to the control (no Mo) encoded hypothetical proteins ($n = 144$), which made it difficult to further assess their importance to *M. maripaludis* physiology as they relate to Mo availability and source. Several of the proteins are hypotheticals with predicted metal binding domains, and these are presented in Supplementary Fig. 9.

Expression of *M. maripaludis* core metabolism genes, including those encoding proteins involved in the methanogenesis pathway (Fmd, Fwd, Ftr, Mch, Hmd, Mer, Mtd, Mtr, Mcr, Hdr; log_2FC range of −0.41 to 0.97 in MoS_4^{2-} vs MoO_4^{2-} cells), formate dehydrogenases involved in formate metabolism (Fdh isoforms 1 and 2; log_2FC range of −0.47 to 0.06 in MoS_4^{2-} vs MoO_4^{2-} cells), and various [NiFe]-hydrogenases involved in H_2 metabolism (Frc/Frh, Vhc/Vhu, and Eha/Ehb; log_2FC range of −0.65 to 0.45 in

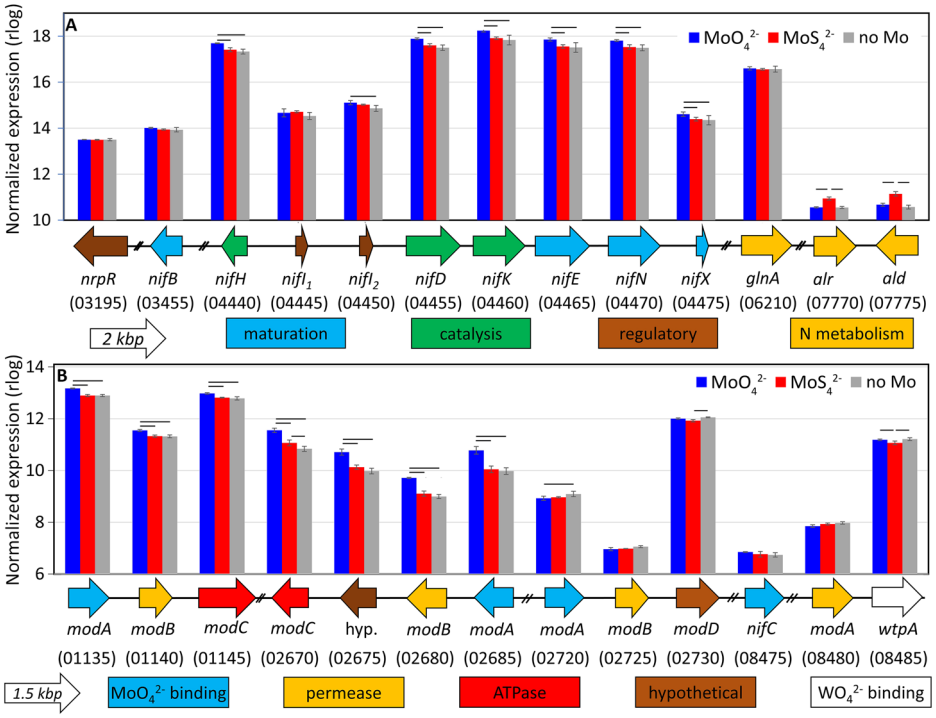

Fig. 5 | Transcriptomic profiles for *Methanococcus maripaludis* S2 cells grown on different molybdenum (Mo) sources under nitrogen-fixing cultivation conditions. Normalized expression values (rlog) are shown for genes encoding proteins directly related to nitrogen fixation or nitrogen metabolism (**A**) or MoO_4^{2-} uptake (*mod* genes) (**B**) in cells provided with molybdate (MoO_4^{2-}, blue bars), tetrathiomolybdate (MoS_4^{2-}, red bars), or no Mo (gray bars). Numbers in parentheses indicate the locus tag (MMP_RSXXXXX) with the "MMP_RS" prefix removed for space. Transcriptional profiles are the average expression values of three replicate cultures. Scale bars and color-coded functions for each gene are shown below each panel. Black bars indicate statistically significant pair-wise comparisons ($p < 0.05$, Wald test).

MoS_4^{2-} vs MoO_4^{2-} cells) generally showed minimal and variable regulation based on the Mo source provided (Supplementary Fig. 10A). This indicated that Mo source did not generally alter the transcriptional regulation of genes involved in cellular energy metabolism. For example, several protein-encoding genes were slightly up-regulated on MoO_4^{2-} (Hmd, Mch), some were slightly up-regulated on MoS_4^{2-} (Fwd, Hdr), and others were slightly up-regulated when no Mo was provided (Mer, Fmd, Mtd) relative to the other conditions, although not necessarily for genes encoding all subunits of a given protein complex. Interestingly, transcription of genes encoding Mo-dependent formylmethanofuran dehydrogenase (Fmd) in cells provided with no Mo was up-regulated relative to cells provided with MoO_4^{2-} or MoS_4^{2-} (which had similar levels of expression). In contrast, transcription of genes encoding the tungsten (W)-dependent formylmethanofuran dehydrogenase (Fwd) was similar in cells provided with MoO_4^{2-} or no Mo but was higher in cells provided with MoS_4^{2-}, suggesting the possibility that W may substitute for Mo in Fwd in MoS_4^{2-}-grown cells. Meanwhile, genes encoding methyl-coenzyme M reductase (Mcr), which catalyzes the final step of methanogenesis, were slightly down-regulated in MoS_4^{2-}-grown cells (log_2FC range of −0.27 to −0.11 in MoS_4^{2-} vs MoO_4^{2-} cells), despite these cultures having the fastest CH_4 production rates.

The expression of genes encoding various [NiFe]-hydrogenases (Frc/Frh, Vhc/Vhu, and Eha/Ehb) was generally similar among the three conditions, although expression of several individual subunits and the entire gene cluster for Ehb showed down expression in cells grown with MoS_4^{2-} relative to those grown with MoO_4^{2-} or no Mo (Supplementary Fig. 10A). Expression of genes encoding Fdh was similar for one isoform (Fdh1; MMP_RS00795-MMP_RS00800) among all culture conditions while expression of genes encoding a second isoform (Fdh2; MMP_RS06680-MMP_RS06685) that is a part of the core methanogenesis gene cluster was higher in MoO_4^{2-}-than MoS_4^{2-}-grown cells (Supplementary Fig. 10B). Interestingly, expression of a gene encoding a formate transporter (FdhC) was higher (log_2FC of 0.21 and 0.50 in MoO_4^{2-}- and MoS_4^{2-}grown cells, respectively) in the no Mo relative to the other conditions potentially due to low growth efficiencies in the no Mo control cells. Genes encoding proteins involved in molybdopterin biosynthesis (Moe and Mog systems[36]) showed little variation in their expression between MoO_4^{2-} and MoS_4^{2-} growth conditions (Supplementary Fig. 11).

Unlike genes encoding components of the *M. maripaludis* energy metabolism that showed minimal regulation based on Mo source, the expression of genes encoding various components of Nif showed more consistent and significant regulation with respect to Mo source (Fig. 5A). For example, differences in the expression of genes encoding the core structural proteins (NifHDK), scaffold proteins (NifEN), and transferase protein (NifX) were among those that most contributed to differences in clustering of transcriptomes along PCO Axis 1. *nifHDKENX* were up-regulated in cells grown with MoO_4^{2-} relative to those grown with MoS_4^{2-} or no Mo. More specifically, expression of *nifH* (log_2fold change = −0.50), *nifD* (−0.52), *nifK* (−0.59), *nifE* (−0.55), *nifN* (−0.51), *and nifX* (−0.39) was down-regulated in MoS_4^{2-}- versus MoO_4^{2-}-grown cells. Genes encoding the radical SAM enzyme, NifB, regulatory proteins (NrpR, $NifI_1I_2$), and glutamine synthetase (GlnA) that is involved in NH_3 assimilation were not differentially regulated in any of the growth conditions tested herein.

M. maripaludis encodes three putative molybdate transport systems (encoded by *mod* operons) and decreased expression of two of these operons (log_2FC range of −0.51 to −0.31 for MMP_RS01135 to MMP_RS01145; and a range of −1.41 to −0.90 for MMP_RS02670 to MMP_RS02685; (Fig. 5B)) in MoS_4^{2-}- versus MoO_4^{2-}-grown cells contributed substantially to differences in clustering of transcriptomes along PCO Axis 1 (Fig. 4A). Expression of genes comprising the third *mod* operon (MMP_RS02720 to MMP_RS02730) did not differ significantly between MoO_4^{2-}- and MoS_4^{2-}-grown cells but was slightly up-regulated in cells not provided with Mo. Other protein-encoding genes predicted to bind Mo, namely a permease (MMP_RS08475) and another *modA* homolog (MMP_RS08480) were not differentially regulated among the growth conditions.

Synthetic molybdenite as a source of Mo

M. maripaludis was tested for its ability to associate with and utilize Mo from MoS_2 to support formatotrophic and diazotrophic growth. Experiments were conducted using 25 μM $FeCl_2$ (rather than FeS_{mack}) with CT or 1 mM HS^- as the S source. Cells were provided with 100 μM synthetic MoS_2 nanoparticles, 5 μM MoO_4^{2-} (positive control), or no Mo added (negative control). Cells grew with MoS_2 as the sole provided Mo source with either CT or with HS^- as S source (Fig. 6A). Production of cells and CH_4 with CT

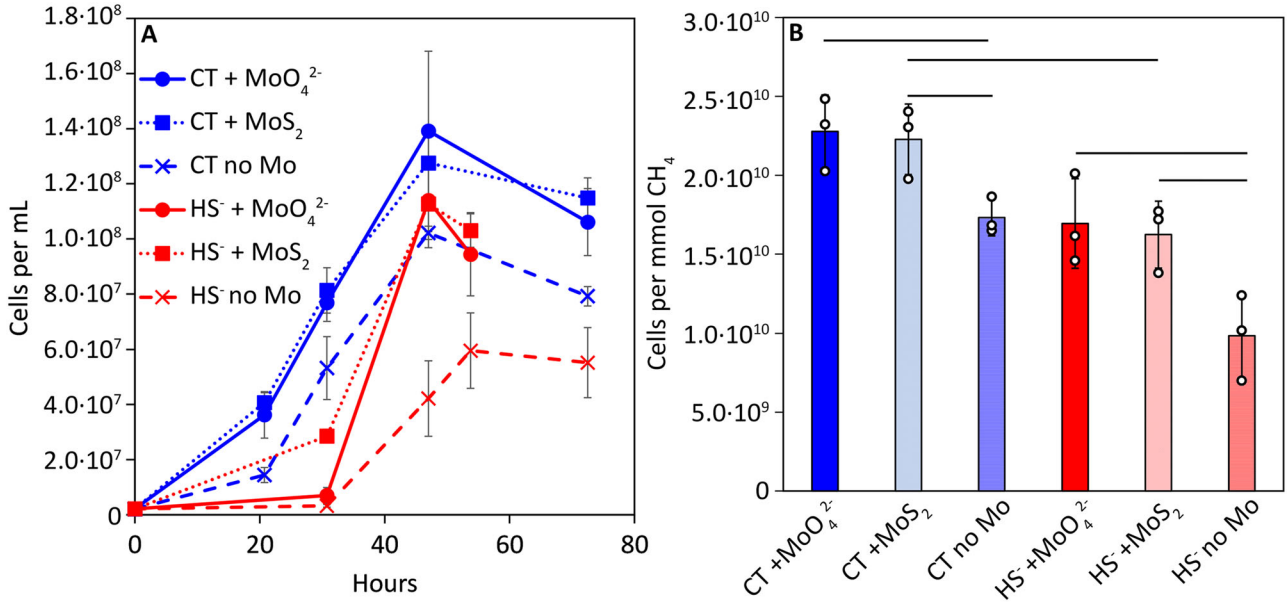

Fig. 6 | Growth of *Methanococcus maripaludis* S2 under nitrogen-fixing cultivation conditions with different molybdenum (Mo) sources in the presence or absence of sulfide. *M. maripaludis* was grown with formate under nitrogen-fixing cultivation conditions with 1 mM each of L-cysteine and thiosulfate (CT, blue series) or 1 mM sulfide (HS^-, red series) as sulfur source and 5 μM molybdate (MoO_4^{2-}, circles), 100 μM (0.0016% w/v) molybdenite (MoS_2, squares), or no molybdenum (no Mo, crosses) as Mo sources. The production of cells was tracked during incubation (**A**). Growth efficiencies were determined using initial cell densities and the number of total cells and the total amount of CH_4 produced before cells reached stationary phase (**B**). Data presented are the mean and standard deviation of three biological replicates per condition. Bars in (**B**) represent statistically significant differences ($p < 0.05$) as determined by two-tailed Student's *t*-tests. The production of CH_4 in these cultures is presented in Supplementary Fig. 12.

as an S source was similar when cultures were provided with MoS_2 or with MoO_4^{2-} (Fig. 6A, Supplementary Fig. 12). Negative control cultures provided with CT but without Mo were able to grow but achieved lower cell densities than those provided with MoS_2 or MoO_4^{2-}. In cultures provided with HS^- as S source, the lag phase was shorter in cultures provided with MoS_2 compared to MoO_4^{2-} (Fig. 6A). Calculation of the number of cells produced per mol of CH_4 reveals that cells grown with CT were more efficient at coupling methanogenesis to cell production than those grown with HS^- (Fig. 6B). The number of cells produced per mmol of CH_4 produced in *M. maripaludis* cultures grown with MoS_2 and MoO_4^{2-} were similar when provided with CT or HS^-, both of which were significantly higher than the no Mo control cultures. Taken together, these results indicate that *M. maripaludis* can acquire Mo from MoS_2.

To better understand the requirement for physical contact with MoS_2 to support growth of *M. maripaludis*, MoS_2 was sequestered in dialysis tubing (12–14 kDa pore size) in the presence of either CT or HS^- as S source, and growth kinetics were compared to cells provided with free access to MoS_2 or to those not provided with Mo. The kinetics of CH_4 production were faster in all CT conditions relative to HS^-, regardless of how Mo was provided to cells (Fig. 7A). However, the efficiency of coupling methanogenesis to growth was highest in cultures allowed direct contact with MoS_2. When allowed direct contact with MoS_2, CT-grown cultures had much higher efficiencies of coupling methanogenesis to cell production than those grown with HS^- (Fig. 7B, Supplementary Fig. 13). In sulfidic conditions where MoS_2 was sequestered, there was a small yet significant stimulation of growth over the no Mo control.

To assess the solubility of synthetic MoS_2 in growth experiments with *M. maripaludis*, 100 μM (0.0016% w/v) of synthetic MoS_2 nanoparticles were incubated in Tris-HCl buffered (pH 7.0) trace metal-free water in the presence or absence of 1 mM HS^-. Subsamples were taken just after MoS_2 addition and after 4 days incubation of the MoS_2 nanoparticles at room temperature (~23 °C). Samples were collected, filtered (0.22 μm, PTFE membrane), and acidified while in an anaerobic glove box and were then subjected to ICP-MS. Low levels of Mo (2 nM) were present in reactors that contained only Tris buffer at the start of the experiment. Similarly, reactors that were amended with HS^- only, MoS_2 only, and MoS_2 plus HS^- contained 3 nM, 25 nM, and 15 nM Mo, respectively, at the start of the experiment (Supplementary Fig. 14). Following 4 days incubation, the amount of Mo in solution increased to 4 nM, 43 nM, and 28 nM in reactors containing HS^- only, MoS_2 only, and MoS_2 plus HS^-, respectively. Thus, HS^- suppresses the abiotic dissolution of MoS_2. Further, of the 100 μM MoS_2 provided, between 0.03% and 0.04% of the Mo was solubilized and able to pass through the 0.22 μm filter over the course of the 4-day incubation.

Natural (specimen) molybdenite as a source of Mo

Given the stimulatory effect of synthetic MoS_2 nanoparticles (<2 μm sieved) on growth of *M. maripaludis*, larger natural specimens of MoS_2 were examined for their ability to support growth. The specimen MoS_2 that was used was not sieved and was ~0.5 cm in diameter. Thus, a greater amount of mineral (0.1% w/v or ~6 mM if it was completely dissolved) was provided to cultures to account for the lower surface area relative to the synthetic MoS_2 nanoparticles. Growth was compared in cultures provided with 5 μM MoO_4^{2-} as the positive control and cultures not provided with Mo as the negative control with either 1 mM CT or HS^- as the provided S source(s). Under CT conditions, cultures provided with MoS_2 and MoO_4^{2-} grew nearly identically in terms of CH_4 and cell production (Supplementary Fig. 15A, C) and both achieved higher cell densities than the negative control. In the presence of HS^-, the MoS2-grown cultures produced more cells and had faster CH_4 production than cultures provided with MoO_4^{2-} or no Mo (Supplementary Fig. 15B, D). These observations were like those observed in cultures provided with synthetic MoS_2 (Fig. 6, Supplementary Fig. 12).

Field-emission scanning electron microscopy (FEM) of glutaraldehyde-fixed *M. maripaludis* cells grown with direct access to MoS_2 under CT or HS^- conditions was performed to observe the cell-mineral interface. CT-grown cells provided with synthetic MoS_2 were sometimes found attached to mineral grains (Fig. 7C), whereas attachment to MoS_2 was common in cultures grown with HS^- (Fig. 7D). Putative vesicles were also observed in association with the MoS_2 surface but were more abundant in the HS^- growth condition than the CT growth condition (Fig. 7D). Cells

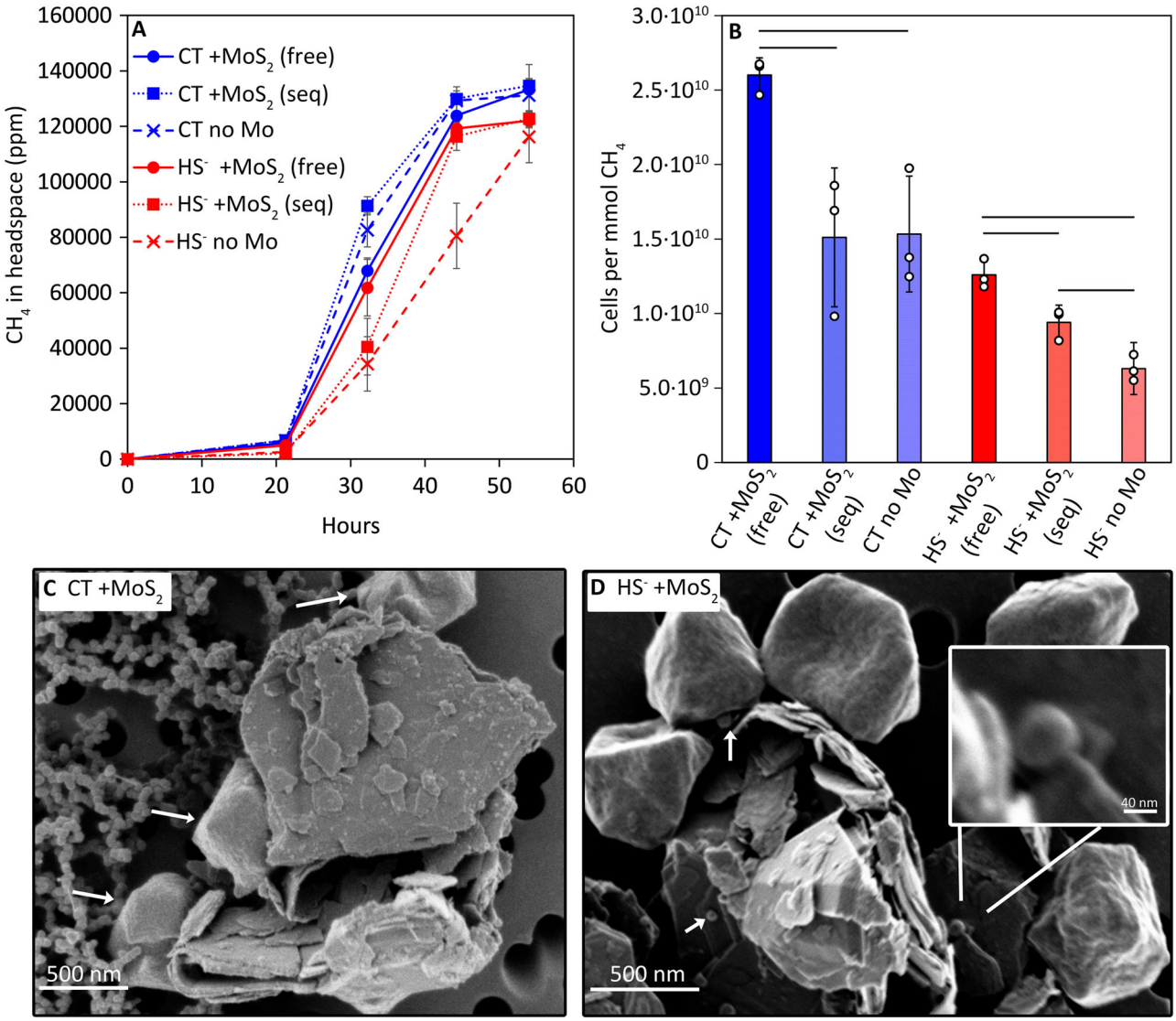

Fig. 7 | Growth of *Methanococcus maripaludis* S2 with or without direct contact to synthetic molybdenite (MoS_2) in the presence or absence of sulfide. *M. maripaludis* was grown with formate under nitrogen-fixing cultivation conditions with 1 mM each of L-cysteine and thiosulfate (CT, blue series) or 1 mM sulfide (HS^-, red series) as sulfur source. MoS_2 was provided free in solution (free, circles), was sequestered in dialysis tubing (seq, squares), or was not provided (no Mo, crosses). The production of cells (Supplementary Fig. 13) and methane (CH_4) (**A**) was tracked during incubation and cells were quantified to determine growth efficiencies (**B**). Field-emission scanning electron micrographs for cells grown with direct contact with MoS_2 and provided with CT (**C**) or HS^- (**D**) show cells and putative vesicles associated with the mineral. White arrows in (**C**) depict *M. maripaludis* cells while white arrows in (**D**) highlight putative vesicles. Data presented are the mean and standard deviation of three replicate cultures per condition. Bars in (**B**) denote statistically significant ($p < 0.05$) pairwise comparisons as determined by two-tailed Student t-tests.

physically associated with specimen MoS_2, with CH_4 bubbles often forming on MoS_2 surfaces resulting in the flotation of the large mineral-biofilm aggregates (Supplementary Fig. 16A, C; Supplementary Movie 1). Electron microscopy of *M. maripaludis* cells grown with specimen MoS_2 grains also showed clear evidence of biofilms associated with the mineral, with more robust or extensive biofilms observed on the specimen MoS_2 for both CT and HS^- conditions in comparison to synthetic MoS_2. Like the synthetic MoS_2, biofilm formation tended to be more extensive on specimen MoS_2 in HS^--grown cultures than CT-grown cultures (Fig. S16 B, D). Energy dispersive electron spectroscopy (EDS) showed increased C and N content relative to the background of MoS_2 in FEMs where cells appeared to be present (Supplementary Fig. 17). Together, these data confirm that cells directly interact with MoS_2 surfaces and show that CT and HS^- conditions affect cellular phenotype with respect to biofilm formation and potentially vesicle formation.

Discussion

Archean oceans were anoxic and limited in Mo, with concentrations in oceans estimated to be as low as 1 nM [3]. Yet, the Last Universal Common Ancestor of Bacteria and Archaea is inferred to have been Mo-dependent[37]. However, the only form of Mo known to be bioavailable is MoO_4^{2-} generated by the O_2-dependent oxidative weathering of MoS_2 and other Mo-bearing minerals in the Earth's crust[4]. The unique redox properties of Mo to catalyze two-electron and oxygen transfer reactions by cycling through Mo(IV) and Mo(VI) redox states enables the oxidation (or reduction) of key substrates[13], such as geologically produced formate[38]. This raises the question, how did early-evolving Mo-dependent cells during the Archean acquire Mo when the availability of Mo (as MoO_4^{2-}) would have been highly limited?

Initial clues to reconcile this paradox came from a previous study of nitrogen-fixing, formate-grown *M. maripaludis* cultures, conditions that

increased the cellular demand for Mo. *M. maripaludis* was shown to grow better and to require less MoO_4^{2-} when grown with FeS_2 than with Fe(II) and HS^- as Fe and S sources[28]. HS^- has a high affinity for Mo and drives the progressive replacement of oxygen atoms in MoO_4^{2-} with S atoms (from HS^-) to form MoS_4^{2-} but only at high HS^- to Mo ratios[29,31,39]. This has been referred to as the "geochemical switch" where Mo exists as MoO_4^{2-} in oxic and low HS^- (<10 μM) environments and MoS_4^{2-} in anoxic and high HS^- (>10 μM) environments[31,40]. However, this geochemical switch is not only applicable to Mo, it also affects the speciation and solubility of a variety of thiophilic metals of relevance to methanogens, including iron, cobalt, nickel, and zinc among others[40–42]. With this in mind, three explanations were put forth to explain the slower growth and higher MoO_4^{2-} requirements of *M. maripaludis* when grown with Fe(II)/HS^- versus FeS_2: (i) low (nM) concentrations of MoO_4^{2-} remain present even in conditions with excess HS^- that are sufficient for growth, (ii) MoS_4^{2-} can meet the Mo demands of cells, or (iii) decreased growth in euxinic conditions is due to HS^- toxicity and/or its effects on the availability of other metals. In the present study, we aimed to test these hypotheses without the confounding influence of HS^- on MoO_4^{2-} speciation with the intent of reconciling the Mo paradox for anaerobes.

Previous studies have shown that *M. maripaludis* can grow with L-cysteine or thiosulfate as S source but only when small amounts of either HS^- (70 μM) or 2-mercaptoethanol are also provided[43]. Consistent with an ability to grow with cysteine, cell lysates of *M. maripaludis* have been shown to exhibit cysteine desulfurase activity despite the genome not encoding homologs of canonical cysteine desulfurase enzymes (i.e., SufS, IscS, NifS)[44,45]. To the authors' knowledge, *M. maripaludis* has not been previously reported to reduce thiosulfate. Nonetheless, here, it was shown that *M. maripaludis* could grow with a combination of L-cysteine and thiosulfate (CT) as S sources. The use of washed cells discounted the likelihood of carryover effects of S sources from the inoculum. Further, very little HS^- (<8 μM) was detected during the CT-dependent growth of *M. maripaludis* (Supplementary Fig. 2C), allowing MoO_4^{2-} to remain stable which enabled a reliable comparison between MoO_4^{2-} and MoS_4^{2-} provided cells.

M. maripaludis cultures were provided with formate as methanogenesis substrate and were required to fix nitrogen with Nif, the only nitrogenase encoded in the genome[34,46]. Together, these growth conditions were sought to force a high Mo demand on cells. With CT as the S source, cultures of *M. maripaludis* were shown to grow as well or better with MoS_4^{2-} when compared to MoO_4^{2-} and UV-Vis spectroscopy confirmed that these Mo species remained stable and in solution during the course of the incubation. Importantly, the amount of Mo per unit biomass was similar among MoS_4^{2-}- and MoO_4^{2-}-grown cells and was significantly ($p < 0.03$) greater in these cells when compared to cells not provided with a Mo source. These observations are consistent with previous studies that have shown Mo limitation to decrease the Mo content of cyanobacterial cultures and to limit nitrogen fixation activity[47]. The faster growth kinetics and similar amounts of Mo in biomass seen here in cultures provided with MoS_4^{2-} relative to MoO_4^{2-} support the use of MoS_4^{2-} by *M. maripaludis* (discounts option i and supports option ii above) and suggest that the negative effect of HS^- on nitrogen-fixing, formate-grown *M. maripaludis* cells is beyond MoO_4^{2-} thiolation alone (option iii above). Collectively, these results are consistent with geochemical arguments indicating that MoS_4^{2-} should be the predominant form of soluble Mo in the sulfidic environments[29,31,40] typically inhabited by methanogens and suggest that MoS_4^{2-} is bioavailable to cells in these environments.

The overall similarity in the growth kinetics of *M. maripaludis* when provided with MoS_4^{2-} versus MoO_4^{2-} prompted a transcriptomic analysis to identify potential differences in the acquisition and trafficking of these forms of Mo in cells. Transcriptomes of *M. maripaludis* grown with soluble MoO_4^{2-}, MoS_4^{2-}, or no added Mo revealed distinct physiological states at the transcriptional level, with two *mod* transporter operons (ModABC) putatively involved in MoO_4^{2-} acquisition[48] among the most differentially expressed genes between MoO_4^{2-}- and MoS_4^{2-}-grown cells. It should be noted, however, that while significant ($p < 0.05$), the changes were subtle, with only 22 genes in the whole genome of *M. maripaludis* showing large log_2FCs between conditions in their RNA abundances ($log_2FC > 1$ or < -1). This is potentially consistent with previous investigations of Mod transporter regulation that have shown that the expression of these systems is generally constitutive with regulation occurring primarily post-transcriptionally[49]. However, in many nitrogen-fixing Bacteria (e.g., *Azotobacter vinelandii*[50]), *mod* transcription can be coordinated with transcription of Nif genes and impairment of *mod* significantly decreases nitrogen fixation in other Bacteria (e.g., *Anabaena variabilis*[51]) (as reviewed in ref. 52). In the methanogen, *Methanosarcina acetivorans*, Mo transport is post-translationally regulated by trans-inhibition of the ModBC transporter through allosteric control by the metal oxyanion[49,53]. Previous transcriptomes of *M. maripaludis* cells provided with MoO_4^{2-} and either FeS_2 or Fe(II)/HS^- as Fe and S source showed that all three of the *mod* gene clusters were strongly up-regulated ($log_2FC\ 2 > X < 6$) under nitrogen-fixing conditions relative to those amended with NH_3[28]. In the present study, the log_2FC of significantly differentially regulated Mod genes ranged from only 0.23–1.4 between cells from MoO_4^{2-} and MoS_4^{2-} conditions. This suggests that the primary cue for regulation of these genes is fixed nitrogen availability, with the source of Mo (MoO_4^{2-} versus MoS_4^{2-}) adding a secondary (albeit small) level of regulation on the first two *mod* gene clusters (MMP_RS01135-MMP_RS01145 and MMP_RS02670-MMP_RS02685).

The differential regulation of Mod transporters in cells grown with MoO_4^{2-} versus MoS_4^{2-}, combined with similar Mo content in biomass, suggests potential overlap in mechanisms of acquiring these anions. Mod has been shown to function in the acquisition of MoO_4^{2-} and the structurally similar anion $WO_4^{[2-49}$, and the allosteric regulation of Mod in *M. acetivorans* can be modulated by either MoO_4^{2-} or $WO_4^{[2-53}$. It is worth noting that the size of MoS_4^{2-} anions is estimated to be only ~20% larger than MoO_4^{2-} due to S forming longer bonds with Mo than oxygen, potentially suggesting that Mod can also transport MoS_4^{2-}. It is also important to note that mechanisms other than Mod must be involved in Mo acquisition in Bacteria and Archaea since ~11% of Mo-utilizing microorganisms (as determined by their genomes encoding Mo-co-dependent enzymes or Nif) are predicted to not encode homologs of the Mod system[15,54]. In our data set, 144 hypothetical proteins were among the most differentially expressed, suggesting some of these genes could be involved in Mo uptake and metallocluster biosynthesis. Thus, it is possible, if not likely, that alternative MoO_4^{2-} and/or MoS_4^{2-} transport systems have yet to be discovered.

Transcriptomes of MoO_4^{2-}-grown cells revealed slight up-regulation of *nifHENX* that encode proteins involved in maturation of the Fe_8S_9C double cubane (NifB-co) core precursor to FeMo-co, enabling nitrogen fixation via Nif[12,55]. This may suggest that MoO_4^{2-} provided cells have a higher demand for FeMo-co maturation proteins than MoS_4^{2-} cells, which may be due to MoS_4^{2-} readily binding Fe-S clusters. Support for this comes from abiotic experiments where MoS_4^{2-}, Fe(II), and HS^- were mixed, resulting in the formation of aqueous Fe-Mo-S cuboidal clusters[56]. These reactions can also occur to produce Mo-Fe-S cubanes on FeS_2[32]. Recent work has begun to show that Fe-Mo-S clusters are able to bind and activate N_2 when supported by organic ligands[57]. Interestingly, the gene encoding the radical SAM enzyme, NifB, which generates NifB-co[58,59], was not differentially regulated in any of the growth conditions tested herein. This may be consistent with NifB having a role in methanogens in addition to its role in FeMo-co biosynthesis, as has been recently reported[60].

NifEN is the scaffold where Mo is added to form the Fe_7MoS_9C precursor to FeMo-co[55]. In Bacteria, NifQ is thought to be the Mo carrier for addition to the Fe_7MoS_9C precursor, however, high concentrations of cysteine in growth medium (a source of HS^- via the activity of cysteine desulfurase) can restore activity in mutant *nifQ* cells[61]. This suggests that MoO_4^{2-} undergoes sulfidation (conversion to a $MoO_{(4-n)}S_n^{2-}$ or even MoS_4^{2-}) either enzymatically (e.g., via cysteine desulfurase in combination with NifQ) or non-enzymatically (e.g., abiotic chemistry) prior to its addition to the Fe_7MoS_9C precursor. Indeed, electron paramagnetic resonance spectroscopy of NifQ indicates that it carries a [Mo-Fe_3-S_4] cluster, and that

it is likely transferred to the Fe_7MoS_9C precursor on a NifHEN complex[62] prior to addition of homocitrate[63] via the activity of homocitrate synthase (NifV). *M. maripaludis* does not encode NifQ or NifV[16] and thus it is possible that MoO_4^{2-} sulfidation is accomplished abiotically via endogenous HS^- (e.g., cysteine desulfurase activity) or via exogenous HS^- that equilibrates with the intracellular environment[64,65]. Importantly, a HS^- concentration of only >10 μM is needed to drive sulfidation of MoO_4[29]. In contrast, MoS_4^{2-} is already fully coordinated by S^{2-} and therefore is more similar to the coordination environment of Mo in FeMo-co (three S, two oxygen, and one nitrogen ligand)[13]. Indeed, decomposition of FeMo-co has been shown to yield tetrathiomolybdate[66]. While spectroscopic studies of FeMo-co in methanogens have yet to be conducted to confirm the presence of homocitrate, homocitrate can be replaced by citrate yielding an enzyme with no N_2 reduction activity in *nifV* mutant Bacteria[67]. Further, other organic acids can substitute for homocitrate in FeMo-co but with decreased N_2 reduction activity[68]. The mechanism of sulfidation of Mo during FeMo-co biosynthesis and the presence and identity of the organic ligand coordinating FeMo-co in methanogens are open and intriguing questions.

Genes encoding components of the molybdopterin cofactor biosynthesis pathway were also not significantly differentially regulated in cells grown with MoS_4^{2-} or MoO_4^{2-}. The molybdo(tungsto)pterin cofactors in Fdh and Fmd/Fwd from methanogens are likely coordinated by 4 cis-dithiolene S atoms of the molybdopterin guanine dinucleotide cofactor and by selenocysteine[14,69]. Like FeMo-co, this makes the coordination environment of Mo in Fdh/Fmd/Fwd molybdopterin (Mo-co) cofactors more similar to that of MoS_4^{2-} than MoO_4^{2-} and indicates that MoO_4^{2-} must be sulfidated prior to its incorporation into Mo-co in *M. maripaludis*. To the authors' knowledge, current pathways for molybdopterin cofactor biosynthesis do not invoke enzymatic sulfidation and it is possible that this process is driven by abiotic chemical reactions with HS^- in Mo-co as well FeMo-co.

M. maripaludis was shown to also be capable of using Mo ions, clusters, or complexes solubilized from MoS_2 to meet its Mo demands. This was not entirely surprising given recent reports that the anaerobe *Clostridium kluyveri* could use MoS_2 as its sole source of Mo to support dinitrogen-dependent growth[10]. However, in addition to Nif, *C. kluyveri* encodes the iron (Anf) and vanadium (Vnf) forms of nitrogenase[70]. Thus, it is possible that *C. kluyveri* decreased its demand for Mo by switching to Anf or Vnf, which is common during Mo limitation[71–73]. Thus, the high dependence on Mo for Fdh, Fmd, and Nif function in *M. maripaludis* without alternative enzyme systems (exception being Fmd/Fwd isoforms) provides additional evidence that solubilized Mo ions, clusters, or complexes from the surface of MoS_2 can be used to meet the Mo demand of methanogens and other anaerobes. While MoS_2 is effectively insoluble, it is possible that surface defects or imperfections allow for increased dissolution. Abiotic dissolution of synthetic MoS_2 showed low amounts (15–43 nM) of Mo could be solubilized from the mineral. However, HS^- suppressed dissolution of Mo from MoS_2, which is consistent with other studies that have shown that the solubility of MoS_2 is inversely correlated with HS^- concentration[74–76]. This suggests the possibility that the Mo that was solubilized from the surface of the synthetic Mo used here (and possibly with *C. kluyveri*) was partially oxidized or contained defects that increased its solubility. While it is not clear what form of Mo is dissolving from the surface of MoS_2, growth data presented here suggests that it is assimilated by *M. maripaludis* and is shifting the equilibrium towards further mineral dissolution. Indeed, binding of Mo by siderophores has been shown to influence Mo dissolution from silicates through a similar effect[77].

Conclusion

Observations presented here indicate that *M. maripaludis* cells can acquire Mo in thiolated forms (i.e., MoS_4^{2-} and MoS_2) that are geochemically relevant to their environment. The use of MoS_4^{2-} did not significantly shift the energy metabolism of *M. maripaludis* nor did it significantly alter the expression of Mo-containing enzymes (e.g., Nif, Fdh, Fmd). Methanogens and other anaerobes characteristically inhabit anoxic and often sulfidic (euxinic) environments and have done so since early in Earth's history[23,24]. The limited availability of MoO_4^{2-} in anoxic environments prior to oxidative weathering of sulfide minerals (as reviewed[3,5]) has long been used to suggest that Mo-dependent enzymes could not have originated at a time prior to oxygenic photosynthesis. Despite this, various molybdoenzymes including Fdh, Fmd, and Nif are thought to have evolved at a time prior to the widespread oxygenation of Earth[26,78–80]. The enhanced growth kinetics, equivalent amounts of Mo in biomass, and similar expression of known pathways of Mo transport in *M. maripaludis* cultures grown with MoS_4^{2-} versus MoO_4^{2-} suggests that MoS_4^{2-} is likely to be the preferred source of Mo for methanogens and other anaerobes. These findings shed new light on the origin and evolution of these molybdoenzymes and help to resolve the Mo paradox, wherein sources of Mo other than MoO_4^{2-} were likely used by the first molybdoenzyme-encoding anaerobes, and also help explain how modern organisms access Mo in anoxic, sulfidic conditions.

Materials and methods

Mineral preparation and characterization

Molybdenite (MoS_2) nanoparticles (<2 μm diameter, CAS: 1317-33-5, Sigma-Aldrich) and specimen MoS_2 (~0.1 to 1.5 cm flakes; Henderson Mine, Colorado, U.S.A.) were transferred in an anaerobic chamber into a 50 mL centrifuge tube and were washed by centrifugation (1000 × *g*; 10 min, 4 °C) with N_2−purged and anoxic solutions according to the following series: Two washes in 18.2 MΩ MilliQ-treated water (MQ H_2O), two washes in 1 M HCl, and three washes in sterile, anoxic MQ H_2O. The resulting pellet for synthetic MoS_2 was resuspended in sterile, anoxic MQ H_2O and the slurry was transferred to a sterile serum bottle, while the specimen MoS_2 was stored dried. The headspace of the serum bottle was flushed with 0.2 μm-filtered N_2 for 15 min to remove residual H_2 from sealing the bottle in the anaerobic chamber that had a < 5% H_2 atmosphere. The concentration of the MoS_2 slurry (wt/v%) was determined by drying three aliquots under N_2 gas and weighing the dried mineral. The dried minerals were then used for XRD analysis with a Bruker D8 Advance Powder X-ray diffractometer to determine the purity of both forms of the MoS_2 (Supplementary Fig. 18). XRD analysis was performed in the JADE software package (Materials Data Inc.).

Cultivation of *M. maripaludis*

M. maripaludis was grown under N_2-fixing conditions in defined basal medium as previously described[28]. To minimize background Mo in medium and culture assays, all glassware and utensils were acid-washed using 50% trace metal grade nitric acid in a chemical fume hood and rinsed three times with MQ H_2O. Optima-grade water was used for medium and stock solution preparation, and PTFE plastic tubing pre-soaked in a 100 mM EDTA (room temperature, >24 h) was used to sparge medium and stock solutions. All medium and stock solution preparation was performed in a chemical (plastic-coated) fume hood that was pre-washed with a citranox acid detergent (Alconox) and wiped with 10% HCl followed by MQ H_2O prior to use.

All solutions were sparged with N_2 gas in sealed serum or medium bottles using plastic tubing at a gas station. For reagents that were O_2-sensitive, solutions were prepared in an anaerobic chamber (95:5 N_2:H_2, Coy) with anoxic Optima water (trace-metal grade for ICP-MS). This included the preparation of ammonia tetrathiomolybdate ($(NH_4)_2MoS_4$) and L-cysteine HCl stock solutions. Growth was typically conducted in 75 mL of media contained in 165 mL serum bottles, or 20 mL of media contained in 70 mL serum bottles. Serum bottles were sealed with new butyl rubber stoppers that were boiled three times in MQ H_2O and were capped within the anaerobic chamber. The headspaces of the serum bottles were flushed with 80:20 N_2:CO_2 and serum bottles and their contents were then autoclaved.

M. maripaludis was provided with 0.4% w/v sodium formate, 10 mM acetate, and Wolfe's vitamins[28]. However, the composition of our trace metals solution was modified to exclude molybdate and ferrous iron; sodium molybdate or $(NH_4)_2MoS_4$ was added separately to a final

concentration of 5 μM. Ferrous iron was added in the form of synthetic mackinawite (FeS_{mack}), which has previously been shown to support growth[81] to a final concentration of 10 μM. In the case of MoS_2 experiments, Fe was provided as $FeCl_2$ to a final concentration of 25 μM. Where specified, HS^- was added to a final concentration of 1 mM, or a mixture of sodium thiosulfate and L-cysteine was added as S source to final concentrations of 1 mM each. All cultures were incubated at 37 °C and over-pressurized with 2.04 atm of 80:20 N_2:CO_2.

M. maripaludis was passaged five times (2% v/v inoculum; ~3×10^8 total cells in 75 mL) in medium without Mo to induce Mo limitation prior to use as an inoculum. Prior to use as inoculum, cultures for use as inoculum were washed by addition of 5 mM nitriloacetic acid[82] and by shaking at ~200 rpm on a rotor shaker (10 min) before centrifugation at 4696 × *g* for 20 min at room temperature. Culture supernatant was removed via a sterile plastic serological pipette in an anaerobic chamber. The cell pellet was then resuspended in basal medium lacking Mo and the cell density was determined immediately prior to inoculation (1% v/v for most experiments).

Quantification of growth

Activity and growth were determined by quantifying headspace CH_4 concentration and cell density. CH_4 concentrations were determined using an SRI gas chromatograph as described previously[81] or using a Shimadzu GC-2014 instrument equipped with a Haysep Q column with ultra-high-purity N_2 as the carrier gas and a TCD detector. For cell concentration determinations, subsamples of culture were fixed in 2.5% glutaraldehyde for 4 h. at 4 °C. Cells were then centrifuged at 15,000 x *g* for 20 min at 4 °C and the supernatant was removed. Cells were resuspended in basal medium prior to cell enumeration with a Petroff-Hausser cell counting chamber via bright-field microscopy[28].

Chemical analyses

Transformations of molybdate or tetrathiomolybdate were tracked using UV-Visible spectroscopy in 20 mL of basal medium in a 70 mL serum bottle with stock additions as described in the main text. The reactors were incubated and pressurized with N_2:CO_2. All samples and standards were prepared by filtering one mL of sample using a 13 mm 0.2 μm PTFE syringe filter into disposable methacrylate cuvettes with a 1 cm pathlength that was capped with polyethylene cuvette stoppers within an anaerobic chamber. Samples were then immediately placed into a Genesys 150 spectrophotometer and assayed using the "scan" function from 280 to 520 nm with 2 nm increments. Standards of molybdate and tetrathiomolybdate were prepared fresh and added in cuvettes in an anaerobic chamber and were sealed before removal from the chamber for analysis. All scans were run against an MQ H_2O blank.

Mass spectroscopy of biomass and supernatants

Quantitative analysis of Mo of digested biomass or supernatant filtrate of abiotic reactors was done on an Agilent 7800 inductively coupled plasma mass spectrometer (ICP-MS) in helium mode. To prepare cells for ICP-MS, they were harvested anaerobically via centrifugation at 4696 × *g* for 20 min at 4 °C and washed three times in 5 mM nitriloacetic acid dissolved in basal medium. After the final wash, the supernatant was removed, and the cells were resuspended in basal medium and transferred into pre-weighed microcentrifuge tubes. The cells were then centrifuged (15,000 x *g* for 15 mins, 4 °C) and the supernatant removed. The cell pellets were then dried overnight using a heat-block at 60 °C with the tubes open and covered with a clean Kimwipe to prevent dust from contaminating the samples while drying. After drying, the weight of the tubes was determined to quantify the biomass. The biomass was then dissolved in 1 mL of 15% trace-metal grade HNO_3 acid at 98 °C overnight with periodic mixing by vortex. After dissolving, the sample was diluted to 3% HNO_3 with Optima H_2O and filtered into a clean tube (0.22 μm, PTFE). For abiotic MoS_2 reactors, supernatant was sampled from the top of the reactors which was then filtered (0.22 μm, PTFE) into 15 mL centrifuge tubes and frozen. Prior to analysis the MoS_2 filtrates were acidified to 3% HNO_3.

Acidified filtrates were analyzed on an Agilent 7800 ICP-MS equipped with a MicroMist nebulizer (Agilent), SPS4 autosampler (Agilent), and x-lens (Agilent). The instrument operating conditions were as follows: RF power, 1600 W; RF matching, 1.8; nebulizer gas, 0.68 L/min; option gas, 0.0%; nebulizer pump speed, 0.10 rps; S/C temp, 2 °C; makeup gas, 0.27 L/min; extract 1 lens, 0.0 V; extract 2 lenses, −195 V; omega bias, −80 V; omega lens, 8.8 V; cell entrance, −40 V; cell exit, −60 V; deflect, 1.4 V, plate bias, −55 V, helium flow rate, 5.0 mL/min; octupole bias, −18 V; octupole RF, 200 V; and energy discrimination, 5.0 V. Concentrations were determined using an 8 point standard curve (Environmental calibration standard, CPI International) ranging from 0.1 to 500 ppb using yttrium as an internal standard (Internal Standard Mix, Agilent). Data acquisition and analysis were done in Agilent MassHunter 4.6 (version C.01.06).

Transcriptomics

Cultures of *M. maripaludis* were harvested during late log phase (24 h. for MoO_4^{2-} and MoS_4^{2-} conditions, 30 h. for no Mo condition) of growth for RNA extraction. Cultures were brought into an anaerobic chamber and were vacuum-filtered over 0.2 μm Supor (Cytiva) membrane filters that were then transferred into 2 mL microcentrifuge tubes. The tubes and their contents were immediately flash-frozen in liquid nitrogen and stored at −80 °C. Total RNA was extracted from the filters using the Trizol method as described previously[28]. DNA contamination was checked by performing PCR amplification using archaeal-specific 16S rRNA primers. The RNA was sent to the University of Wisconsin's Genome Expression Center for quality control, rRNA depletion using custom *Methanococcus*-specific oligonucleotides[28], and sequencing on an Illumina NovaSeq 2 × 150 bp (Illumina, San Diego, CA). RNA paired-end reads were processed to remove adapter sequences and filter reads using TrimGalore! (v.0.6.6) before reads were aligned to the reference *M. maripaludis* genome with Bowtie2 to generate transcriptional profiles as previously reported[28]. Briefly, the mapped reads to the *M. maripaludis* genome were enumerated with the HT-Seq and statistically analyzed using the DESeq2 package for R. A single outlier transcriptome was removed from each treatment based on significant deviation from the other three biological replicate profiles. The RNA-sequencing data reported in this paper have been deposited in the NCBI GEO database (GSE261517).

Dialysis experiments

To separate cells from MoS_2, 12–14 kDa dialysis tubing (SpectraPor, Repligen) was loaded (within an anaerobic chamber) with the equivalent amount of synthetic MoS_2 slurry used to grow cells that had direct contact. Before use, the tubing was first cleaned by incubating it twice in MQ H_2O at 60 °C for 2 h. followed by a third incubation in 50% ethanol. The tubing was then rinsed with anoxic MQ H_2O in an anaerobic chamber and was loaded with MoS_2 via mechanical micropipette. The tubing was sealed with plastic clips that had been modified to fit into serum bottles and the outside of the tubes and clips were rinsed with anoxic MQ H_2O. Pre-prepared growth reactors containing medium were then opened in the anaerobic chamber and the tubing was added and the reactors resealed. After all reactors had either empty tubing (positive and negative controls) or filled tubing (experimental condition) added, they were inoculated and the headspace of the reactors was immediately flushed for 15 min with 0.2 μm of 80:20 N_2:CO_2 to remove chamber H_2. The reactors were then incubated statically on their sides at 37 °C.

Electron microscopy

Field-emission scanning electron microscopy (FE-SEM) was used to visualize *M. maripaludis* cells. The cells were first fixed in glutaraldehyde (see above) and dehydrated for 5 min at each concentration of an ethanol series of 50%, 70%, 80%, 90%, 95%, and 100% using a microfiltration and vacuum apparatus. For cells grown with specimen MoS_2, 50% electron microscopy-grade glutaraldehyde was injected into mid-log phase culture bottles to a final concentration of 2.5 v/v%. The culture bottles were then placed at 4 °C overnight. The medium was then carefully poured off, leaving

the MoS_2 grains in the bottle. Phosphate-buffered saline was then added to the bottles, allowed to incubate for 15 min at 4 °C, and then poured off to remove residual glutaraldehyde. The cells or MoS_2 grains were filtered onto Au-sputtered 0.2 µm polycarbonate filters (Millipore, Sigma) and air-dried within a petri dish. After drying, the filters (synthetic MoS_2 cultures) or specimen MoS_2 grain were mounted onto FE-SEM sample pegs using double-sided carbon (C) tape. For the MoS_2 grains, clean forceps were used to place the grains directly onto the C tape. Samples were then coated with iridium via sputtering for 1 min with a 20 mA current. The cells were then imaged at the Imaging and Chemical Analysis Laboratory at Montana State University using a high-resolution Supra 55VP electron microscope (Zeiss, Thornwood, NY) with a primary electron beam energy of 1 keV at different magnifications. Elemental mapping was performed with a 15 keV beam energy and an Ultim Max energy-dispersive x-ray spectrometer (Oxford instruments) and analyzed in the AZtec software package.

Statistics and reproducibility

All data shown are mean values of at least three independent biological replicates, with error bars denoting the standard deviation, unless indicated otherwise in the figure caption. Statistical analyses for cell growth data were performed in Microsoft Excel using the two-way t-test assuming unequal variance, with the p-value for the two-way t-test reported as significant when $p < 0.05$. For transcriptomics data, significance differences reported are the adjusted p-value from the Wald test calculated in the DEseq2 package.

Reporting summary

Further information on research design is available in the Nature Portfolio Reporting Summary linked to this article.

Data availability

All data generated or analyzed during this study are included in the text and figures of this published article and its Supplementary Materials. Sequencing data from transcriptomics experiments are available through the NCBI Gene Expression Omnibus under the accession ID GSE261517. Additionally, processed transcriptomic data can be found in Supplementary Data File 1. Data from growth studies and abiotic experiments are provided separately in Supplementary Data File 2. All other data are available from the corresponding author upon reasonable request.

Received: 1 July 2024; Accepted: 10 October 2024;
Published online: 16 October 2024

References

1. Shock, E. L. & Boyd, E. S. Principles of geobiochemistry. *Elements* **11**, 395–401 (2015).
2. Collier, R. W. Molybdenum in the Northeast Pacific Ocean. *Limnol. Oceanogr.* **30**, 1351–1354 (1985).
3. Anbar, A. D. Elements and evolution. *Science* **322**, 1481–1483 (2008).
4. Scott, C. et al. Tracing the stepwise oxygenation of the Proterozoic ocean. *Nature* **452**, 456–459 (2008).
5. Anbar, A. D. & Knoll, A. H. Proterozoic ocean chemistry and evolution: a bioinorganic bridge? *Science* **297**, 1137–1142 (2002).
6. Williams, R. J. & Fraústo da Silva, J. J. The involvement of molybdenum in life. *Biochem. Biophys. Res. Commun.* **292**, 293–299 (2002).
7. Falkowski, P. G. Evolution of the nitrogen cycle and its influence on the biological sequestration of CO_2 in the ocean. *Nature* **387**, 272–275 (1997).
8. Schoepp-Cothenet, B. et al. The ineluctable requirement for the trans-iron elements molybdenum and/or tungsten in the origin of life. *Sci. Rep.* **2**, 263 (2012).
9. Paerl, H. W., Crocker, K. M. & Prufert, L. E. Limitation of N_2 fixation in coastal marine waters: relative importance of molybdenum, iron, phosphorus, and organic matter availability. *Limnol. Oceanogr.* **32**, 525–536 (1987).
10. Sheng, Y. et al. Mineral-bound trace metals as cofactors for anaerobic biological nitrogen fixation. *Environ. Sci. Technol.* **57**, 7206–7216 (2023).
11. Lancaster, K. M. et al. X-ray emission spectroscopy evidences a central carbon in the nitrogenase iron-molybdenum cofactor. *Science* **334**, 974–977 (2011).
12. Seefeldt, L. C., Hoffman, B. M. & Dean, D. R. Mechanism of Mo-dependent nitrogenase. *Annu. Rev. Biochem.* **78**, 701–722 (2009).
13. Schwarz, G., Mendel, R. R. & Ribbe, M. W. Molybdenum cofactors, enzymes and pathways. *Nature* **460**, 839–847 (2009).
14. Niks, D. & Hille, R. Molybdenum- and tungsten-containing formate dehydrogenases and formylmethanofuran dehydrogenases: Structure, mechanism, and cofactor insertion. *Protein Sci.* **28**, 111–122 (2019).
15. Zhang, Y. & Gladyshev, V. N. Molybdoproteomes and evolution of molybdenum utilization. *J. Mol. Biol.* **379**, 881–899 (2008).
16. Boyd, E. S. et al. Evolution of molybdenum nitrogenase during the transition from anaerobic to aerobic metabolism. *J. Bacteriol.* **197**, 1690–1699 (2015).
17. Bertram, P. A., Schmitz, R. A., Linder, D. & Thauer, R. K. Tungstate can substitute for molybdate in sustaining growth of *Methanobacterium thermoautotrophicum*. Identification and characterization of a tungsten isoenzyme of formylmethanofuran dehydrogenase. *Arch. Microbiol.* **161**, 220–228 (1994).
18. Schmitz, R. A., Albracht, S. P. & Thauer, R. K. A molybdenum and a tungsten isoenzyme of formylmethanofuran dehydrogenase in the thermophilic archaeon *Methanobacterium wolfei*. *Eur. J. Biochem.* **209**, 1013–1018 (1992).
19. Halim, M. F. A., Day, L. A. & Costa, K. C. Formate-dependent heterodisulfide reduction in a *Methanomicrobiales* archaeon. *Appl. Environ. Microbiol.* **87**, e02698–02620 (2021).
20. Kurth, J. M., Op den Camp, H. J. M. & Welte, C. U. Several ways one goal—methanogenesis from unconventional substrates. *Appl. Microbiol. Biotechnol.* **104**, 6839–6854 (2020).
21. Dos Santos, P. C., Fang, Z., Mason, S. W., Setubal, J. C. & Dixon, R. Distribution of nitrogen fixation and nitrogenase-like sequences amongst microbial genomes. *BMC Genomics* **13**, 162 (2012).
22. Boyd, E. & Peters, J. New insights into the evolutionary history of biological nitrogen fixation. *Front. Microbiol*. **4**, 201 (2013).
23. Ueno, Y., Yamada, K., Yoshida, N., Maruyama, S. & Isozaki, Y. Evidence from fluid inclusions for microbial methanogenesis in the early Archaean era. *Nature* **440**, 516–519 (2006).
24. Wolfe, J. M. & Fournier, G. P. Horizontal gene transfer constrains the timing of methanogen evolution. *Nat. Ecol. Evol.* **2**, 897–903 (2018).
25. Russell, M. J. & Martin, W. The rocky roots of the acetyl-CoA pathway. *Trends Biochem. Sci.* **29**, 358–363 (2004).
26. Boyd, E. S. et al. A late methanogen origin for molybdenum-dependent nitrogenase. *Geobiology* **9**, 221–232 (2011).
27. Liu, Y., Beer, L. L. & Whitman, W. B. Methanogens: a window into ancient sulfur metabolism. *Trends Microbiol.* **20**, 251–258 (2012).
28. Payne, D., Spietz, R. L., Newell, D. L., Dijkstra, P. & Boyd, E. S. Influence of sulfide on diazotrophic growth of the methanogen *Methanococcus maripaludis* and its implications for the origin of nitrogenase. *Commun. Biol.* **6**, 799 (2023).
29. Erickson, B. E. & Helz, G. R. Molybdenum(VI) speciation in sulfidic waters: stability and lability of thiomolybdates. *Geochim. Cosmochim. Acta* **64**, 1149–1158 (2000).
30. Phillips, R. & Xu, J. A critical review of molybdenum sequestration mechanisms under euxinic conditions: Implications for the precision of molybdenum paleoredox proxies. *Earth-Sci. Rev.* **221**, 103799 (2021).
31. Helz, G. R. et al. Mechanism of molybdenum removal from the sea and its concentration in black shales: EXAFS evidence. *Geochim. Cosmochim. Acta* **60**, 3631–3642 (1996).
32. Bostick, B. C., Fendorf, S. & Helz, G. R. Differential adsorption of molybdate and tetrathiomolybdate on pyrite (FeS_2). *Environ. Sci. Technol.* **37**, 285–291 (2003).

33. Helz, G. R., Vorlicek, T. P. & Kahn, M. D. Molybdenum scavenging by iron monosulfide. *Environ. Sci. Technol.* **38**, 4263–4268 (2004).
34. Kessler, P. S., McLarnan, J. & Leigh, J. A. Nitrogenase phylogeny and the molybdenum dependence of nitrogen fixation in *Methanococcus maripaludis*. *J. Bacteriol.* **179**, 541–543 (1997).
35. Laurie, StuartH. Thiomolybdates—simple but very versatile reagents. *Eur. J. Inorg. Chem.* **2000**, 2443–2450 (2000).
36. Iobbi-Nivol, C. & Leimkühler, S. Molybdenum enzymes, their maturation and molybdenum cofactor biosynthesis in *Escherichia coli*. *Biochim. Biophys. Acta* **1827**, 1086–1101 (2013).
37. Zerkle, A. L., House, C. H. & Brantley, S. L. Biogeochemical signatures through time as inferred from whole microbial genomes. *Am. J. Sci.* **305**, 467–502 (2005).
38. McDermott, J. M., Seewald, J. S., German, C. R. & Sylva, S. P. Pathways for abiotic organic synthesis at submarine hydrothermal fields. *Proc. Natl Acad. Sci. USA* **112**, 7668 (2015).
39. Harmer, M. A. & Sykes, A. G. Kinetics of the interconversion of sulfido- and oxomolybdate(VI) species $MoO_xS_{4-x}^{2-}$ in aqueous solutions. *Inorg. Chem.* **19**, 2881–2885 (1980).
40. Rickard, D. & Morse, J. W. Acid volatile sulfide (AVS). *Mar. Chem.* **97**, 141–197 (2005).
41. Luther, G. W. & Rickard, D. T. Metal sulfide cluster complexes and their biogeochemical importance in the environment. *J. Nanopart. Res.* **7**, 389–407 (2005).
42. Rickard, D., Luther, G. W., I. I. I. Metal sulfide complexes and clusters. *Rev. Mineral. Geochem.* **61**, 421–504 (2006).
43. Rajagopal, B. S. & Daniels, L. Investigation of mercaptans, organic sulfides, and inorganic sulfur compounds as sulfur sources for the growth of methanogenic bacteria. *Curr. Microbiol.* **14**, 137–144 (1986).
44. Liu, Y., Sieprawska-Lupa, M., Whitman, W. B. & White, R. H. Cysteine is not the sulfur source for iron-sulfur cluster and methionine biosynthesis in the methanogenic archaeon *Methanococcus maripaludis*. *J. Biol. Chem.* **285**, 31923–31929 (2010).
45. Johnson, C. et al. Pathways of iron and sulfur acquisition, cofactor assembly, destination, and storage in diverse archaeal methanogens and alkanotrophs. *J. Bacteriol*. **203**, https://doi.org/10.1128/jb.00117-00121 (2021).
46. Kessler, P. S., Blank, C. & Leigh, J. A. The *nif* gene operon of the methanogenic archaeon *Methanococcus maripaludis*. *J. Bacteriol.* **180**, 1504–1511 (1998).
47. Tuit, C., Waterbury, J. & Ravizza, G. Diel variation of molybdenum and iron in marine diazotrophic cyanobacteria. *Limnol. Oceanogr.* **49**, 978–990 (2004).
48. Grunden, A. M. & Shanmugam, K. T. Molybdate transport and regulation in bacteria. *Arch. Microbiol.* **168**, 345–354 (1997).
49. Ma, Z., Jacobsen, F. E. & Giedroc, D. P. Coordination chemistry of bacterial metal transport and sensing. *Chem. Rev.* **109**, 4644–4681 (2009).
50. Hamilton, T. L. et al. Transcriptional profiling of nitrogen fixation in *Azotobacter vinelandii*. *J. Bacteriol.* **193**, 4477–4486 (2011).
51. Zahalak, M., Pratte, B., Werth, K. J. & Thiel, T. Molybdate transport and its effect on nitrogen utilization in the cyanobacterium *Anabaena variabilis* ATCC 29413. *Mol. Microbiol.* **51**, 539–549 (2004).
52. Demtröder, L., Narberhaus, F. & Masepohl, B. Coordinated regulation of nitrogen fixation and molybdate transport by molybdenum. *Mol. Microbiol.* **111**, 17–30 (2019).
53. Gerber, S., Comellas-Bigler, M., Goetz, B. A. & Locher, K. P. Structural basis of trans-inhibition in a molybdate/tungstate ABC transporter. *Science* **321**, 246–250 (2008).
54. Peng, T., Xu, Y. & Zhang, Y. Comparative genomics of molybdenum utilization in prokaryotes and eukaryotes. *BMC Genomics* **19**, 691 (2018).
55. Hu, Y. & Ribbe, M. W. Biosynthesis of the metalloclusters of nitrogenases. *Annu. Rev. Biochem.* **85**, 455–483 (2016).
56. Vorlicek, T. P. et al. Molybdenum burial mechanism in sulfidic sediments: Iron-sulfide pathway. *ACS Earth Space Chem.* **2**, 565–576 (2018).
57. McSkimming, A. & Suess, D. L. M. Dinitrogen binding and activation at a molybdenum–iron–sulfur cluster. *Nat. Chem.* **13**, 666–670 (2021).
58. Wiig, J. A., Hu, Y., Lee, C. C. & Ribbe, M. W. Radical SAM-dependent carbon insertion into the nitrogenase M-cluster. *Science* **337**, 1672–1675 (2012).
59. Curatti, L., Ludden, P. W. & Rubio, L. M. NifB-dependent in vitro synthesis of the iron-molybdenum cofactor of nitrogenase. *Proc. Natl Acad. Sci. USA* **103**, 5297–5301 (2006).
60. Jasleen, S., Ahmed, D., Abaranjitha, M., Andrew, J. A. & Daniel, J. L. The nitrogenase cofactor biogenesis enzyme NifB is essential for the viability of methanogens. *bioRxiv*, 2023.2010.2020.563283 (2023).
61. Ugalde, R. A., Imperial, J., Shah, V. K. & Brill, W. J. Biosynthesis of the iron-molybdenum cofactor and the molybdenum cofactor in *Klebsiella pneumoniae*: effect of sulfur source. *J. Bacteriol.* **164**, 1081–1087 (1985).
62. Rubio, L. M. & Ludden, P. W. Biosynthesis of the iron-molybdenum cofactor of nitrogenase. *Annu. Rev. Microbiol.* **62**, 93–111 (2008).
63. Rangaraj, P. & Ludden, P. W. Accumulation of 99Mo-containing iron-molybdenum cofactor precursors of nitrogenase on NifNE, NifH, and NifX of *Azotobacter vinelandii*. *J. Biol. Chem.* **277**, 40106–40111 (2002).
64. Mathai, J. C. et al. No facilitator required for membrane transport of hydrogen sulfide. *Proc. Natl Acad. Sci. USA* **106**, 16633–16638 (2009).
65. Lee, J. K. et al. Structural basis for conductance by the archaeal aquaporin AqpM at 1.68 Å. *Proc. Natl Acad. Sci. USA* **102**, 18932–18937 (2005).
66. Newton, W. E. et al. Elicitation of thiomolybdates from the iron-molybdenum cofactor of nitrogenase. *Eur. J. Biochem.* **159**, 111–115 (1986).
67. Mayer, S. M., Gormal, C. A., Smith, B. E. & Lawson, D. M. Crystallographic analysis of the MoFe protein of nitrogenase from a *nifV* mutant of *Klebsiella pneumoniae* Identifies citrate as a ligand to the molybdenum of iron molybdenum cofactor (FeMoco). *J. Biol. Chem.* **277**, 35263–35266 (2002).
68. Imperial, J., Hoover, T. R., Madden, M. S., Ludden, P. W. & Shah, V. K. Substrate reduction properties of dinitrogenase activated in vitro are dependent upon the presence of homocitrate or its analogs during iron-molybdenum cofactor synthesis. *Biochemistry* **28**, 7796–7799 (1989).
69. Wagner, T., Ermler, U. & Shima, S. The methanogenic CO_2 reducing-and-fixing enzyme is bifunctional and contains 46 [4Fe-4S] clusters. *Science* **354**, 114–117 (2016).
70. Seedorf, H. et al. The genome of *Clostridium kluyveri*, a strict anaerobe with unique metabolic features. *Proc. Natl Acad. Sci. USA* **105**, 2128–2133 (2008).
71. Joerger, R. D., Jacobson, M. R., Premakumar, R., Wolfinger, E. D. & Bishop, P. E. Nucleotide sequence and mutational analysis of the structural genes (anfHDGK) for the second alternative nitrogenase from *Azotobacter vinelandii*. *J. Bacteriol.* **171**, 1075–1086 (1989).
72. Joerger, R. D. et al. Nucleotide sequences and mutational analysis of the structural genes for nitrogenase 2 of *Azotobacter vinelandii*. *J. Bacteriol.* **172**, 3400–3408 (1990).
73. Oda, Y. et al. Functional genomic analysis of three nitrogenase isozymes in the photosynthetic bacterium *Rhodopseudomonas palustris*. *J. Bacteriol.* **187**, 7784–7794 (2005).
74. Zhang, L., Audétat, A. & Dolejš, D. Solubility of molybdenite (MoS_2) in aqueous fluids at 600–800°C, 200MPa: A synthetic fluid inclusion study. *Geochim. Cosmochim. Acta* **77**, 175–185 (2012).
75. Cao, X. *Solubility of molybdenite and the transport of molybdenum in hydrothermal solutions*. (Iowa State University, 1989).
76. Agapova, G. F., Shmariovich, Y. M., Vorob'yev, I. M. & Khitarov, D. N. Experimental study of the behavior of molybdenum in hot sulfide-carbonate solutions. *Int. Geol. Rev.* **29**, 491–498 (1987).

77. Liermann, L. J., Guynn, R. L., Anbar, A. & Brantley, S. L. Production of a molybdophore during metal-targeted dissolution of silicates by soil bacteria. *Chem. Geol.* **220**, 285–302 (2005).
78. Adam, P. S., Borrel, G. & Gribaldo, S. An archaeal origin of the Wood–Ljungdahl H_4MPT branch and the emergence of bacterial methylotrophy. *Nat. Microbiol.* **4**, 2155–2163 (2019).
79. Weiss, M. C., Preiner, M., Xavier, J. C., Zimorski, V. & Martin, W. F. The last universal common ancestor between ancient Earth chemistry and the onset of genetics. *PLoS Genet.* **14**, e1007518 (2018).
80. Stüeken, E. E., Buick, R., Guy, B. M. & Koehler, M. C. Isotopic evidence for biological nitrogen fixation by molybdenum-nitrogenase from 3.2 Gyr. *Nature* **520**, 666–669 (2015).
81. Payne, D., Spietz, R. L. & Boyd, E. S. Reductive dissolution of pyrite by methanogenic archaea. *ISME J.* **15**, 3498–3507 (2021).
82. Edgcomb, V. P. et al. Sulfide ameliorates metal toxicity for deep-sea hydrothermal vent archaea. *Appl. Environ. Microbiol.* **70**, 2551–2555 (2004).

Acknowledgements

We thank Sara Zacher for her expertize and training to facilitate electron microscopy and X-ray diffraction that was performed at the Imaging and Chemical Analysis Laboratory (ICAL), a Montana Nanotechnology Facility, a National Nanotechnology Infrastructure Center member. This work was supported by the Division of Chemical Sciences, Geosciences, and Biosciences, Office of Basic Energy Sciences of the U.S. Department of Energy through Grant DE-SC0020246 (BB, ESB).

Author contributions

Conceptualization: D.P., E.S.B., Methodology: D.P., J.L., L.M.K., D.R.C., Investigation: D.P., J.L., L.M.K., Visualization: D.P., J.L., D.R.C., Supervision: E.S.B., B.B., Writing—original draft: D.P., E.S.B., Writing—review & editing: D.P., L.M.K., D.R.C., J.L., B.B., E.S.B.

Competing interests

The authors declare no competing interests.

Additional information

Supplementary information The online version contains supplementary material available at https://doi.org/10.1038/s42003-024-07049-w.

Correspondence and requests for materials should be addressed to Eric S. Boyd.

Peer review information *Communications Biology* thanks the anonymous reviewers for their contribution to the peer review of this work. Primary Handling Editors: Xiaoling Xu and Tobias Goris. A peer review file is available.